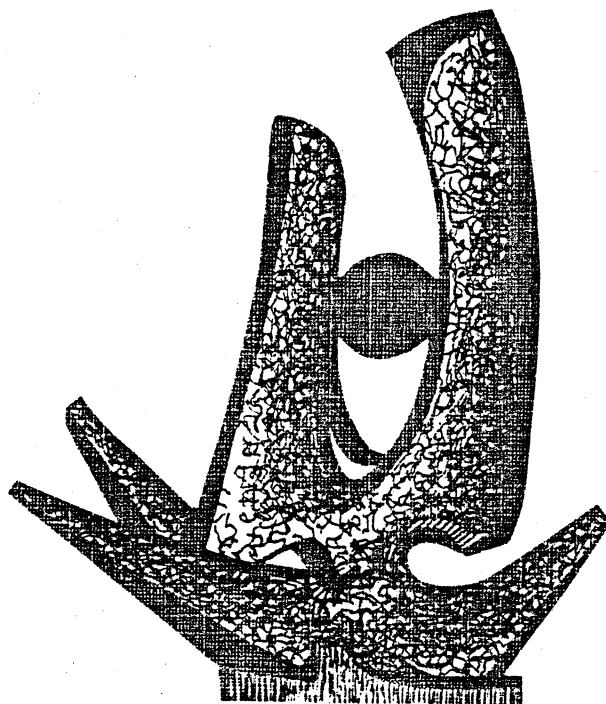


MICHIGAN STATE UNIVERSITY

CYCLOTRON LABORATORY

E2 CORE POLARIZATION FOR SD SHELL SINGLE-PARTICLE  
STATES CALCULATED WITH A SKYRME-TYPE INTERACTION

H. SAGAWA and B.A. BROWN



MARCH 1984

MSUCL-453



E2 CORE POLARIZATION FOR SD SHELL SINGLE-PARTICLE STATES  
CALCULATED WITH A SKYRME-TYPE INTERACTION

H. Sagawa and B. A. Brown  
Cyclotron Laboratory  
Michigan State University  
East Lansing, MI 48824-1321

Abstract: We have studied the core-polarization effect on the  $1s0d$  shell single-particle electromagnetic quadrupole transitions due to coupling with the quadrupole giant resonances. The self-consistent Hartree-Fock + RPA method is applied for the calculations of the single-particle wave functions and the response functions of the giant resonances. The particle-vibration coupling model is used to calculate the core-polarization effect in the vicinity of  $^{16}O$  and  $^{40}Ca$ . The effective coupling Hamiltonian is determined by the SGI Skyrme-type interaction which is used in the H-F + RPA and particle-vibration coupling calculation. The results are discussed for the proton and neutron effective charges and for the longitudinal and transverse form factor for the  $0d_{3/2}^{-1} \rightarrow 1s_{1/2}^{-1}$  proton single-particle transition in  $^{39}K$ . Good agreement with recent longitudinal data for this transition is obtained.

I. Introduction

Electron scattering is a powerful method for studying the density and current distributions in both the ground state and in transitions to the excited nuclear states. The longitudinal form factors are determined by the density distributions. The transverse form factor gives us also information about the current distribution. Shell-model calculations, carried out within a model space consisting of the nucleons being restricted to occupy a few orbits near the Fermi surface, have been compared with the experimental longitudinal quadrupole ( $C_2$ ) form factors of nuclei over a broad region of the mass table [some recent references are (Ref 1) for the  $sd$  shell, (Ref 2) for the  $fp$  shell and (Ref 3) for  $^{90}Zr$ ]. However, the comparison for the strong transitions always shows that the theoretical form factors at the first maximum as well as the gamma decay transition probabilities are smaller (typically by about a factor of four) than experiment. Empirically this has been taken care of by introducing "effective charges" for the protons and neutrons. Much theoretical work has been done in order to understand the microscopic origin of these effective charges. Their magnitudes can be qualitatively understood by the coherent mixing of the  $1p-1h$  "giant quadrupole" excitation into the low lying states. This effect can be regarded as a polarization of the core protons by the valence protons and neutrons (Ref 4) and is often referred to as the

"core-polarization" effect. We will use the expression "core-polarization" charge to describe this component of the total "effective" charge.

Microscopic calculations must be carried out in order to obtain the full momentum transfer dependence of the longitudinal effective charge as well as to obtain the analogous correction for the transverse form factor. Such a calculation must be able to successfully describe the properties of both the ground state single-particle wave functions and the giant quadrupole resonance, and it must also describe the coupling between these two states. The key ingredient for all of these calculations is the nuclear interaction which is used. The appropriate interaction is not easy to arrive at since the free nucleon-nucleon interaction itself must be renormalized to take into account the model-space truncation. Our approach in this work is to consistently use a phenomenological interaction which has been designed to successfully reproduce many of the ground state and giant resonance state properties of the closed-shell nuclei over a wide mass region. All aspects of our calculations are carried out using the a Skyrme-type interaction. It is in this way that our work differs from previous work on the calculations of electron scattering form factors which have used finite-range two-body interactions (Ref 5 and Ref 6) and schematic two-body interactions (Ref 7 and Ref 8).

In particular, we have used the SGII Skyrme interaction. (Ref 9 and Ref 10). This interaction has several advantages over previous Skyrme-type interactions. It keeps reasonable ground state properties, while having a lower compression modulus of  $K_{\infty} = 215$  MeV (Ref 9). It also gives realistic properties for the giant resonances including the spin-isospin modes (Ref 10). Moreover, the SGII interaction has an attractive pairing matrix element for the particle-particle type two-body correlation. These improvements are mainly due to the introduction of a lower power of the density dependence and a modification of the spin-exchange terms for the velocity dependent parts of the interaction.

We have studied the core-polarization effect on the single-particle electromagnetic transitions based on the self-consistent Hartree-Fock (H-F) and the random phase approximation (RPA) theory. We first calculate the single-particle wave functions using the Skyrme-type effective interaction and the RPA response function is also obtained by using the same interaction. The core-polarization is taken into account by the particle-vibration coupling model. We will describe a summary of RPA response function theory and the formulas for the perturbation calculation in the section II. The numerical results for the single-particle transitions in the vicinity of  $^{40}\text{Ca}$  are discussed in the section III. A summary is given in the section IV.

## II. Formulation

### II-a) RPA response function calculation

Starting from the time dependent Hartree-Fock theory (TDHF), we can derive the RPA Green's function as a small amplitude approximation (Ref 11);

$$\begin{aligned} \text{GRPA}(\underline{r}_1, \underline{r}_2; E) &= G_0(\underline{r}_1, \underline{r}_2; E) \\ &+ \int \text{GRPA}(\underline{r}_1, \underline{r}'; E) V_{ph}(\underline{r}') G_0(\underline{r}', \underline{r}_2; E) d\underline{r}' \end{aligned} \quad (1)$$

where  $G_0$  is the unperturbed p-h Green's function,  $V_{ph}$  is the residual p-h interaction and  $E$  is the excitation energy. The unperturbed response  $G_0$  is expressed as

$$\begin{aligned} G_0(\underline{r}_1, \underline{r}_2; E) &= \int_{p, h} \phi_p^*(\underline{r}_1) \phi_p(\underline{r}_1) \\ &\times \{ (\epsilon_p - \epsilon_h - E + i\eta)^{-1} + (\epsilon_p - \epsilon_h + E - i\eta)^{-1} \} \\ &\times \phi_h(\underline{r}_2) \phi_p^*(\underline{r}_2) \end{aligned} \quad (2)$$

where  $\epsilon_h$  and  $\phi_h$  ( $\epsilon_p$  and  $\phi_p$ ) are the energies and wave functions of occupied (unoccupied) Hartree-Fock states calculated with  $V(\underline{r}_1, \underline{r}_2)$ . The symbol  $\int$  in Eq. (2) means summation over discrete states and integration over continuous states.

The sum on particle states can be extended to all particle and

hole states since every hole-hole (h-h) contribution from the first term in the bracket will be cancelled by a corresponding contribution from the second term. This summation on all states can be expressed in a closed form,

$$\begin{aligned} \int_p \phi_p(\underline{r}_1) \{ (\epsilon_p - \epsilon_h - E + i\eta)^{-1} \} \phi_p^*(\underline{r}_2) \\ = \langle \underline{r}_1 | (H_0 - \epsilon_h - E + i\eta)^{-1} | \underline{r}_2 \rangle \end{aligned} \quad (3)$$

where  $H_0$  is the Hartree-Fock Hamiltonian. When one uses the Skyrme-type interaction, Eq. (3) becomes a differential operator equation and is easy to solve numerically (it would be an integro-differential equation for a finite-range interaction). In this way, one can avoid the problem of truncating the particle-hole (p-h) configuration space. Moreover, one can take into account the single-particle continuum effect on the width of the resonance by solving the RPA Green's function in the coordinate space (Ref 12, Ref 9). We require a self-consistent treatment for the calculations of  $G_0$  and  $V_{ph}$ . Both quantities should be obtained from the same two-body interaction  $V(\underline{r}_1, \underline{r}_2)$  in this treatment of the response function.

Once Eq. (1) has been solved for a given excitation energy  $E$ , we can obtain the corresponding excitation strength for a one-body operator  $Q$ . If  $E$  is above the particle emission threshold, the transition strength  $S(E)$  is obtained by

$$S(E) = \sum_n |\langle n | Q | 0 \rangle|^2 \delta(E - E_n) = [1/\pi] \text{Im}[\text{Tr}((Q^\dagger \text{GRPA}(E) Q))] \quad (4)$$

while for bound states below the threshold, the excitation energies and transition strengths appear as real poles and residues in the response function  $\text{Tr}(Q^\dagger \text{GRPA } Q)$ .

Since GRPA behaves in the vicinity of resonance as (Ref 11)

$$\text{Im}[\text{GRPA}(\underline{r}, \underline{r}'; E_{\text{res}})] \approx \delta\rho(\underline{r}) \cdot \delta\rho(\underline{r}'), \quad (5)$$

we can obtain the transition density  $\delta\rho(\underline{r})$  of giant resonance by integrating one of the radial coordinate of GRPA as

$$\delta\rho(\underline{r}) = \alpha \int \text{Im}[\text{GRPA}(\underline{r}, \underline{r}'; E_{\text{res}})] d\underline{r}' \quad (6)$$

where

$$\alpha^2 = B(E_x) / [\pi S(E_{\text{res}})]^2 \quad (7)$$

For an isolated resonance,  $B(E_x)$  is the total integrated strength for the operator  $Q = r^\lambda Y_{\lambda\mu}(\hat{r})$  over the resonance.

The two-body interaction  $V(\underline{r}_1, \underline{r}_2)$  has density-independent terms and a density-dependent term,

$$\begin{aligned} V(\underline{r}_1, \underline{r}_2) = & t_0(1+x_0P_\sigma) \delta(\underline{r}_1 - \underline{r}_2) \\ & + t_1(1+x_1P_\sigma) [(k'^2 + k^2)/2] \delta(\underline{r}_1 - \underline{r}_2) \\ & + t_2(1+x_2P_\sigma) k' \cdot \delta(\underline{r}_1 - \underline{r}_2) k \\ & + [1/6] t_3(1+x_3P_\sigma) \rho^\alpha(R) \delta(\underline{r}_1 - \underline{r}_2) \end{aligned} \quad (8)$$

where  $R = (\underline{r}_1 + \underline{r}_2)/2$ ,  $k = (\underline{\nabla}_1 - \underline{\nabla}_2)/(2i)$  and  $k' = (\underline{\nabla}_1 - \underline{\nabla}_2)/(-2i)$ .

The parameters are selected for having reasonable values for the Landau parameters in comparison with the renormalised G-matrix calculations while keeping realistic properties in the Hartree-Fock calculations (Ref 10). We use the parameter set SG11 for the following calculations since this interaction gives a successful description for various nuclear collective excitations. The residual interaction  $V_{\text{ph}}$  can be derived by taking the second derivative of the energy density for Eq. (8) with respect to densities (Ref 11). This procedure is equivalent to the Landau prescription in the Fermi liquid theory. The p-h interaction is given explicitly as

$$\begin{aligned} V_{\text{ph}} = & \delta^2 E(\rho) / \delta\rho\delta\rho = \delta(\underline{r}_1, \underline{r}_2) \{ a \\ & + b [ \underline{\nabla}_1^2 + \underline{\nabla}_2^2 + \underline{\nabla}_1 \cdot \underline{\nabla}_2 ] \\ & - (\underline{\nabla}_1 - \underline{\nabla}_1') \cdot (\underline{\nabla}_2 - \underline{\nabla}_2') \} \\ & + c (\underline{\nabla}_1 + \underline{\nabla}_1') \cdot (\underline{\nabla}_2 + \underline{\nabla}_2') \} \end{aligned}$$

with

$$\begin{aligned}
 a &= (3/4) t_0 + (3/48) (\alpha + 2) (\alpha + 1) t_3 \rho^\alpha \\
 &- (1/48) t_3 (1+2x_3) \alpha (\alpha-1) \rho^2 t \rho^\alpha / \rho^2 \\
 &- [ (1/4) t_0 (1+2x_0) + (1/24) t_3 (1+2x_3) \rho^\alpha ] \underline{\tau} \cdot \underline{\tau} \\
 b &= - (1/32) \{ 3t_1 + t_2 (5+4x_2) \\
 &+ [ t_2 (1+2x_2) - t_1 (1+2x_1) ] \underline{\tau} \cdot \underline{\tau} \} \\
 c &= (1/32) \{ 3t_1 - 3t_2 (5+4x_2) \\
 &- [ t_1 (1+2x_1) + 3t_2 (1+2x_2) ] \underline{\tau} \cdot \underline{\tau} \}
 \end{aligned}$$

where  $\rho_t = \rho_n - \rho_p$ . In Eq. ( 9 ), the indices 1,1' refer to the p-h coordinates to the left and 2,2' are those to the right. The spin-dependent terms are discarded in Eq. (10).

II-b) Form for the operators in the helicity formalism

In our calculations it is practical to use the helicity representations of the operators and the states in which most of expectation values of one-body operators can be written by using only the Clebsch-Gordan coefficients (Ref 13, Ref 11). The  $\delta$ -type interaction can be transformed into the helicity coordinate by the following simple form;

( 9 )

$$\begin{aligned}
 V(\underline{r}_1, \underline{r}_2) &= \delta(\underline{r}_1 - \underline{r}_2) \underline{\sigma}_1 \cdot \underline{\sigma}_2 \underline{\nabla}_1 \cdot \underline{\nabla}_2 \\
 &= \sum_{\alpha, \beta, \lambda, \mu} [\delta(\underline{r}_1 - \underline{r}_2) / (r_1 \cdot r_2)] (2\lambda + 1) / (4\pi) \\
 &\quad \times \sigma^\alpha 1\alpha \nabla^{*1} \beta^* D^*_{\mu\lambda} \hat{Y}^\alpha(r_1) \\
 &\quad \times D_{\mu\lambda} \hat{Y}^\alpha(r_2) \sigma_2^\alpha \nabla_2 \beta.
 \end{aligned}$$

(11)

where  $\gamma = \alpha + \beta$ . The electromagnetic transition operators are also rewritten to be

(10)

$$\begin{aligned}
 T(\text{CA}) &= \sum_i (1/2 - t_{zi}) f_\lambda(r_i) Y_{\lambda\mu}(\hat{r}_i) \\
 &= \sum_i (1/2 - t_{zi}) f_\lambda(r_i) [(2\lambda + 1) / (4\pi)]^{1/2} \\
 &\quad \times D^{\lambda\mu}_0(\hat{r}_i)
 \end{aligned}$$

(12)

and

$$\begin{aligned}
 T_{\text{spin}}(\text{EA/MA}) &= \sum_i [\lambda(2\lambda + 1)]^{1/2} f_{L\lambda}(r_i) \\
 &\quad \times [g_S(i)/2] [Y_L(\hat{r}_i) X_{\underline{\sigma}_i}]_\lambda \\
 &= \sum_i [(2\lambda + 1) / (4\pi)]^{1/2} f_{L\lambda}(r_i) g_S(i) / 2 \\
 &\quad \times \{ F_1(\lambda) D^{\lambda\mu}_0 \sigma_0 + F_2(\lambda) D^{\lambda\mu}_1 \sigma_{+1} \}.
 \end{aligned}$$

(13)

where  $\lambda = l + / - 1$  corresponds to the transverse magnetic operator, while  $\lambda = l$  corresponds to the transverse electric operator. The convection current contribution to the transverse electric form factor has the same form as Eq. (13) but with  $\underline{\sigma}$  replaced by the operator  $\underline{\nabla} - \underline{\nabla}$  and  $g_S$  replaced by  $g_E$ . Finally the orbital part of the MA operator for  $\lambda = l + / - 1$  is given by

$$T_{\text{Orbit}}(M_{\lambda}) = \sum_i [2g_{\lambda}(i)/(i+1)] f_{\lambda}(r_i) \\ \times [Y_{\lambda}(r_i) \times \hat{J}_{\lambda}]_{\lambda} \\ = [(2\lambda+1)/8\pi]^{1/2} [4g_{\lambda}(i)/(i+1)] f_{\lambda}(r_i) \\ \times F_3(\lambda) D^{\lambda} \mu_{\lambda} \hat{J}_{\lambda+1}$$

(14)

In these equations  $F_1$ ,  $F_2$  and  $F_3$  are given by

$$F_1(\lambda = \lambda-1) = -[\lambda(\lambda+1)]^{1/2} \quad F_2(\lambda = \lambda-1) = (2)^{1/2} \lambda \\ F_1(\lambda = \lambda) = 0 \quad F_2(\lambda = \lambda) = -[2\lambda(2\lambda+1)]^{1/2} \\ F_1(\lambda = \lambda+1) = \lambda \quad F_2(\lambda = \lambda+1) = [2\lambda(\lambda+1)]^{1/2} \\ \text{and} \\ F_3(\lambda = \lambda-1) = \lambda \\ F_3(\lambda = \lambda) = -[\lambda(2\lambda+1)]^{1/2} \\ F_3(\lambda = \lambda+1) = [\lambda(\lambda+1)]^{1/2}$$

(15)

We propagate the operators which are included in the interaction

Eq. (9) in order to calculate GRPA. For spin-independent

excitations, we will take 6 propagators (1,

$$\underline{V}_1^2 + \underline{V}_2^2 + \underline{V}_{1'}^2 + \underline{V}_{2'}^2, (\underline{V}_1 +/\underline{V}_{1'})_0 \text{ and} \\ (\underline{V}_1 +/\underline{V}_{1'})_{+1} \} \times [(2\lambda+1)/4\pi]^{1/2} D^{\lambda} \mu_{\lambda} 0$$

We also have to include spin-dependent propagators  $D^{\lambda} \mu_{\lambda} \alpha_{\pm 1}$  and  $D^{\lambda} \mu_{\lambda} 0$  for calculating the magnetic transition strength

and the electric transverse form factor. Altogether, 8 propagators are taken into account in the response function GRPA.

II-c) Perturbation formulae for the core polarization due to RPA excitations

We use perturbation theory to calculate the core-

polarization effect due to the giant resonances. The modified single-particle wave function is expressed as

$$|\tilde{i}\rangle = |i\rangle + \sum_{j,\lambda,\omega_{\lambda}} \langle(j\lambda\omega_{\lambda})|V_{ph}|i\rangle \\ \times [\epsilon_i - (\epsilon_j + \omega_{\lambda})]^{-1} |(j\lambda\omega_{\lambda})i\rangle$$

(16)

The reduced matrix element for the one-body operator is modified to be (Ref 14, Ref 6)

$$\langle \tilde{j} || T_{\lambda} || \tilde{i} \rangle = \langle j || T_{\lambda} || i \rangle \\ + \sum_{\omega_{\lambda}} [2\omega_{\lambda} / (\epsilon_j)^2 - (\omega_{\lambda})^2] \\ \times \langle V_{ph} \rangle \langle \omega_{\lambda} || T_{\lambda} || 0 \rangle / (2\lambda+1)^{1/2}$$

(17)

where  $\epsilon_{ij} = \epsilon_i - \epsilon_j$ . The major contributions to the residual

interaction  $V_{ph}$  come from  $t_0(1+x_3p_0)$  and

$t_3(1+x_3p_0)\rho^{\alpha}$  and the velocity dependent terms  $t_1$  and

$t_2$  have small contributions for the spin-independent matrix

elements. We take into account the velocity dependent terms in Eq.

(9) by using the Fermi-gas approximation. Then  $V_{ph}$  becomes



$$\begin{aligned}
V_{ph}^{IS}(\underline{r}_1, \underline{r}_2) &= \{ (3/4)t_0 + (3/48)(\alpha+2)(\alpha+1)t_3 \} \rho^\alpha(R) \\
&+ (1/8) k_F^2 [3t_1+t_2(5+4x_2)] \delta(\underline{r}_1-\underline{r}_2) \\
V_{ph}^{IV}(\underline{r}_1, \underline{r}_2) &= \{ -(1/4)t_0(1+2x_0) - (1/24)t_3(1+2x_3) \} \rho^\alpha(R) \\
&+ (1/8) k_F^2 [t_2(1+2x_2) - t_1(1+2x_1)] \delta(\underline{r}_1-\underline{r}_2)
\end{aligned} \tag{18}$$

where the fermi momentum  $k_F$  is taken to be  $1.33 \text{ fm}^{-1}$ . In this approximation, the effect of the velocity dependent terms is to renormalize the  $t_0$  and  $x_0$  to the effective values;

$$t_0^* = -2476.5 \text{ (MeV.fm}^3\text{)}, \quad x_0^* = 0.0478 \tag{19}$$

while the original  $t_0$  and  $x_0$  values of SGII interaction are  $t_0 = -2645 \text{ (MeV.fm}^3\text{)}$  and  $x_0 = 0.09$ . For the simplified interaction of Eq. (18) the isoscalar ( $\beta=IS$ ) and isovector ( $\beta=IV$ ) matrix elements  $\langle V_{ph} \rangle$  can be expressed in a simple form,

$$\begin{aligned}
\langle V_{ph}^\beta \rangle &= \int r^2 dr V_{ph}^\beta(r) \delta\rho_\lambda^\beta \\
&\times R_f(r) R_i(r) \langle f | |Y_\lambda| | i \rangle
\end{aligned} \tag{20}$$

where  $t=1$  for IS and  $t=-r_z$  for IV.  $\delta\rho_\lambda^\beta$  is the transition density of the giant resonance and  $R(r)$  is the radial wave function of the single-particle state.

### III. Results

We show in Fig. (1) the RPA response for the isoscalar (IS) and isovector (IV) quadrupole operators  $r^2 Y_{2\mu}$ ,  $r^2 Y_{2\mu} \tau_z$  in  $^{40}\text{Ca}$ . The IS collective resonance appears as a sharp peak at  $E_x = 16.7 \text{ MeV}$  exhausting 67% of the energy weighted sum rule (EWSR) of  $9084 \text{ MeV-fm}^4$ , while the isovector resonance is spread out in the energy region  $E_x = 25-35 \text{ MeV}$ . The observed IS giant resonance is around  $E_x = 16.7 \text{ MeV}$  and exhausts about 2/3 of EWSR value (Ref 15). The strength function of the IV giant

resonances between 25-35 MeV has about 71% of the isovector EWSR value of  $9084(1+K) \text{ MeV-fm}^4$  where  $K=0.27$  is the enhancement factor for the SG2 interaction (Ref 16). The rest of EWSR value lies in the high energy region and the transition strength itself is very small. We take into account only these strong resonances in the core-polarization calculations since the high energy tail of the strength distribution gives a relatively small contribution. The isoscalar results for  $^{16}\text{O}$  are EWSR =  $2236 \text{ MeV-fm}^4$  with the IS state at  $E_x = 20.3 \text{ MeV}$  exhausting 75% of the EWSR.

The major contribution to the core-polarization comes from the isoscalar resonance and we first discuss this in terms of the isoscalar effective charge. In Table I we give the isoscalar contributions for the 0s-1d single-particle matrix elements for the particle states in  $^{16}\text{O}$  and the hole states in  $^{40}\text{Ca}$ . The

proton and neutron effective charges are based on Eq. (17) with the  $T_\lambda$  operator taken at zero momentum transfer (i.e. with  $f_\lambda(r_j)=r_j^\lambda$ ) and are defined as the ratios

$$\delta e_p = 1 - \langle \tilde{j} || T_\lambda(q=0) || \tilde{i} \rangle_\mu / \langle j || T_\lambda(q=0) || i \rangle_\mu$$

and

$$\delta e_n = \langle \tilde{j} || T_\lambda(q=0) || \tilde{i} \rangle_\nu / \langle j || T_\lambda(q=0) || i \rangle_\nu$$

The individual isoscalar and isovector contributions to these will be denoted by  $\delta e^I_S$  and  $\delta e^I_V$ .

We first discuss the state dependence of the results for  $\delta e^I_S$ . For the degenerate oscillator states it is worthwhile to remember that with a central interaction connecting the particle and vibration that the effective charge is independent of the initial and final total angular momenta  $j_f-j_i$  for a given combination of the orbital angular momenta  $l_f-l_i$  and for a given core (Ref 17). We use a central force but there is still some orbit dependence in our results due to the difference between the H-F and oscillator radial wave functions and to the splitting of the single-particle state via  $\epsilon_{ij}$  in Eq. (17). The effect of  $\epsilon_{ij}$  is to increase the effective charge for the off-diagonal matrix elements relative to the diagonal matrix elements. The effect of the HF radial wave functions is primarily to reduce the value of the core-polarization charge when the nucleons are loosely

bound and have a large mean-square radius.

In (Ref 18) it was argued that the radial wave function dependence of the effective charge is empirically roughly proportional to some power of the ratio  $G$  which is defined as the matrix element of  $r^2$  calculated with the H-F single-particle radial wave functions divided by this matrix element calculated with harmonic-oscillator radial wave functions

$$G = \langle f || r^2 || i \rangle_{HF} / \langle f || r^2 || i \rangle_{HO} \quad (21)$$

These ratios for our calculation are given in Table II. The power depends on the range of the interaction which connects the single-particle state and vibration and varies empirically from about -2 for a zero-range delta interaction to 0 (i.e. the effective charge is independent of the radial wave function) for the long range Q.Q interaction. If we do not include the density dependence in Eq. (18) (and thus have just have a delta interaction) this power in our case is about -1.6 and with the full density dependent interaction the power is closer to about -1.3. Thus the effect of the density dependence is to slightly reduce the state dependence of the effective charge.

The empirical isoscalar effective charge in the mass region A=20-36 has been obtained from a comparison of the experimental  $E_2$

matrix elements with those calculated with the full multi-particle ( $0d_{3/2}$ )<sup>n</sup> wave functions (Ref 18 and Ref 1). Over this mass region the empirical isoscalar effective charge is remarkably state and mass independent with an average value of  $0.35 \pm 0.05$ . To compare this with the results given in Table I we should take into account that the multi-particle matrix elements are dominated by the  $0d_{5/2}-0d_{5/2}$  ( $\delta_{eth}=0.36$ ) and  $0d_{5/2}-1s_{1/2}$  ( $\delta_{eth} = 0.25$ ) terms at the beginning of the shell and by the  $0d_{3/2}-0d_{3/2}$  ( $\delta_{eth}=0.40$ ) term at the end of the shell. The average of the theoretical results given above in brackets is 0.34 in excellent agreement with the empirical value of  $0.35 \pm 0.05$ . It will be interesting in the future to try to extract from the multi-particle data the orbit dependence suggested by the present calculations.

Zamick et al., pointed out that a short-range interaction gives a very large core-polarization charge,  $\delta e_{IS} = 1.71$ , for the quadrupole transition in the case of  $^{40}\text{Ca}$  (Ref 19). We have done also a schematic calculation using only  $t_0(1+x_0)$  and  $t_3(1+x_3)\rho^\alpha$  interactions with the parameters ( $t_0 = -1094$  MeV.fm<sup>3</sup>,  $x_0 = 0.609$ ,  $t_3 = 19750$  MeV.fm<sup>6</sup>,  $x_3 = 1$  and  $\alpha = 1$ ). This parameter set gives a reasonable mean charge radius and binding energy for  $^{40}\text{Ca}$ . However, the energy of IS giant resonance comes down from  $E_x = 17.2$  MeV to  $E_x = 13.0$  MeV and the transition strength is increased from  $B(E2) = 388$  e<sup>2</sup>fm<sup>4</sup> to  $B(E2) = 563$  e<sup>2</sup>fm<sup>4</sup>.

These changes gives the core-polarization charge  $\delta e_{IS} = 1.1$  for the  $(0d_{3/2} \rightarrow 1s_{1/2})_p$  transition instead of  $\delta e_{IS} = 0.45$  coming from the full interaction. The velocity dependent terms  $t_1(1+x_1)$  and  $t_2(1+x_2)$  are crucial to obtain a reasonable energy for the isoscalar giant quadrupole resonance and hence also for the amount of core-polarization charge.

Next we discuss the isovector contribution to the single-hole matrix elements in  $^{40}\text{Ca}$ . The results are given in Table III for the average contribution to the proton and neutron. As can be noted for the  $^{40}\text{Ca}$  isoscalar case in Table I the difference of the individual proton and neutron values from the average is relatively small. The factor of 4 difference between the IS and IV core-polarization charges is due to several effects. The energy dependence  $\omega_\lambda$  in Eq. (17) induces a factor 2 difference between  $\delta e_{IS}$  to  $\delta e_{IV}$  since  $\omega_{IS} = 16.7$  MeV while  $\omega_{IV}$  is at around 30 MeV. Also the  $B(E2)$  value comes out to be a factor 1.6 different, i.e.,  $B(E2) = 388$  e<sup>2</sup>fm<sup>4</sup> for IS case and  $B(E2) = 246$  e<sup>2</sup>fm<sup>4</sup> for IV resonances between  $E_x = 25-35$  MeV. The transition matrices which appear twice in the last term of Eq.(17), i.e., in  $\langle V \rangle$  and  $\langle \omega_\lambda || T_\lambda || 0 \rangle$ , thus give an additional factor of 1.6. Finally there is a factor of about 1.3 difference between the strength of the IS and IV p-h interactions.

The empirical isovector effective charge for the sd shell

nuclei has proved to be difficult to obtain because it is sensitive to what is assumed about the valence radial wave functions (Ref 18). The empirical results range from a value of  $\epsilon_p - \epsilon_n = 1.0$  (the free nucleon value) obtained with a harmonic oscillator potential to a smaller value of  $\epsilon_p - \epsilon_n = 0.35$  obtained with a non-local (energy dependent) Woods-Saxon potential. An intermediate value of  $\epsilon_p - \epsilon_n = 0.67$  was obtained with the local (energy independent) Woods-Saxon potential (Ref 18). Thus for  $\delta e^{1V} = (\epsilon_n - \epsilon_p + 1)/2$  we have a wide range of empirical values from 0 to +0.16 to +0.32. The present result of +0.11 fits in this range and agrees best with the local Woods-Saxon analysis of Ref 18.

A more complete test of our calculations would come from a comparison with experimental electron scattering form factor data for the single-particle transitions  $A=17$  and  $A=39$ . Of course only  $17_0$  and  $39_K$  targets exist and for these only the  $d_{3/2}$  and  $s_{1/2}$  states in  $17_0$  and the  $d_{3/2}$  and  $s_{1/2}$  states in  $39_K$  exist in nature in a relatively pure form, the higher states having fragmented single-particle strength due to the mixing with core excited states. The longitudinal C2 form factors for the elastic transitions are difficult to observe because of the dominant C0 contributions (transverse E2 for the elastic vanishes due to parity conservation). This leaves us with only two inelastic transitions to provide information on the C2 and E2 form factors. Some low-q data for  $39_K$  has existed for some years

(Ref 20) and very recently at NIKHEF medium-q and high-q data has been obtained (Ref 21). In this work we will compare our calculations with these data. Additional comparisons to some of the multi-particle sd shell data (Ref 1) will be part of a future work.

The form factors were calculated starting from the operators for point protons given in Sec. II-b. The center of mass correction was taken into account in the usual harmonic-oscillator approximation (Ref 22). The nucleon finite size corrections were incorporated in the dipole approximation (Ref 13, p.386). The calculations were carried out in the plane wave Born approximation (PWBA). For this small Z value, the PWBA C2 form factor is very close to a DWBA calculation when one takes into account the distortion effect with an effective momentum transfer value  $q_{eff}$ , except in the minima and in the rise just after the minima where the DWBA is filled in relative to PWBA (Ref 1). We compare our PWBA calculation plotted vs.  $q$  to the experimental data plotted vs  $q_{eff}$ .

The Coulomb form factor of the quadrupole transition ( $0d_{3/2}^{-1} \rightarrow 1s_{1/2}^{-1}$ )<sub>p</sub> in  $39_K$  is shown in Fig. (2). The dashed line corresponds to the result without core polarization, while the solid curve shows the result with the core polarization. The calculated transition strength

$B(E2)_{\text{theory}} = 21.1 e^2 \text{fm}^4$  agrees well with the experimental one  $B(E2)_{\text{exp}} = (18.9 \pm 1.8) e^2 \text{fm}^4$  which is obtained at the limit  $q=0$  (Ref 20). The  $q$ -dependence of the form factor is nicely reproduced by the calculation with the core polarization. The calculation shows also quantitative agreement of the absolute magnitudes of the first peak at  $q=0.75 \text{ fm}^{-1}$  and the second peak at  $q = 1.7 \text{ fm}^{-1}$ . One of the aspects of our calculation which is important in obtaining this good agreement, is the fact that the calculated H-F mean square charge radius of  $3.48 \text{ fm}$  for  $^{40}\text{Ca}$  is in agreement with the experimental value of  $3.481 \pm 0.005 \text{ fm}$  Ref 23.

We show in Fig. (3) the transition densities of IS and IV giant resonances together with that of the Tassie model,

$$\delta\rho^\lambda(r) \propto r^{\lambda-1} \frac{d\rho_0(r)}{dr} \quad (22)$$

where  $\rho_0$  is the ground state proton density. The IS transition density is very close to the Tassie-type one, while the IV transition density of the resonance at  $E_x = 29 \text{ MeV}$  changes sign at around  $r = 2 \text{ fm}$ . The other IV resonances have almost the same radial dependences for the transition densities as the state at  $E_x = 29 \text{ MeV}$ . Due to the couplings to these resonances, the transition density for the  $(0d\ 3/2^{-1} \rightarrow 1s1/2^{-1})_{\pi}$  transition is increased at the surface region and decreased slightly in

the inside of the nucleus (see Fig. (4)). This change of the transition density is responsible for the larger enhancement at the first peak than the second peak in the form factor in Fig. (2).

The M1 and E2 transverse form factors for the  $(0d\ 3/2^{-1} \rightarrow 1s1/2^{-1})_{\pi}$  transition are shown in Fig. (5). At the small  $q$ -region, the M1 and E2 form factors have almost same order of magnitude, while the E2 form factor becomes dominant at high  $q$ -region around  $2 \text{ fm}^{-1}$ . The core-polarization effect on the E2 form factor quenches the first peak at  $q = 0.9 \text{ fm}^{-1}$  and does not change much in the second peak. The calculated form factor follows the main feature of the experimental one in high- $q$  region. On the other hand, in the low  $q$ -region, the theory is higher than experiment.

We have not calculated the core-polarization corrections to the M1 form factor since they cannot be carried out as a straightforward generalization of the E2 calculation. Moreover, it is clear for  $q=0$  that delta-isobar admixtures, higher-order nuclear configuration mixing and meson exchange currents are all important for the M1 matrix element (Ref 24) and these effects together with the first-order core polarization should be considered for a complete calculation of the transverse form factor. We should also mention that the tensor force is important for the higher-order nuclear configuration mixing (Ref 24) and is also probably

important for the first-order core-polarization and this Tensor component should be added on to our Skyrme interaction in order to obtain a reliable result for the transverse form factor.

#### IV. Summary

We have studied the core-polarization effect on the electromagnetic transitions in the vicinity of  $^{16}\text{O}$  and  $^{40}\text{Ca}$ . The self-consistent H-F + RPA method was used for the calculations of the single-particle wave functions and the response functions of isoscalar and isovector giant resonances taking the Skyrme-type interaction SGI1. The core-polarization effect was studied by the particle-vibration coupling model using the same Skyrme-type interaction for the coupling Hamiltonian. For the important matrix elements involved in the multi-particle sd shell transitions we obtained an average isoscalar effective charge of  $6eIS = 0.34$  in good agreement with the empirical result of  $0.35 \pm 0.05$  (Ref 18, Ref 1). The calculated isovector effective charge is  $6eIV = 0.11$  which is consistent with the analysis of Ref 18. For the well-bound states in  $^{40}\text{Ca}$  the state dependence of the core-polarization charge is small and at most 20%.

We show in Fig. (2) the Coulomb form factor of the transition  $(0d_{3/2}^{-1} \rightarrow 1s_{1/2}^{-1})_{\pi}$  in  $^{39}\text{K}$ . The calculated form factor shows good agreement with the experimental one both in

the  $q$ -dependence and the absolute magnitudes of the first peak and the second peak. The core-polarization effect on the transverse form factor is shown in Fig. (5). The comparison with experiment is not as good in this case and indicates the need to include delta-isobars, higher-order nuclear configuration mixing and mesonic exchange corrections in the calculation.

#### Acknowledgements:

This research was supported in part by the National Science Foundation Grant No. PHY-83-12245.

## Figure Captions:

Fig. (1) The response functions for the isoscalar and isovector quadrupole transitions in  $^{40}\text{Ca}$ . The solid and dashed curves correspond to the IS and IV excitations, respectively. For the purpose of presentation the response functions are averaged over a Gaussian shape with the width of 1 MeV. (The calculated decay width of the isoscalar state is about 200 keV.)

Fig. (2) The Coulomb form factor of the quadrupole transition  $(0d_{3/2}^{-1} \rightarrow 1s_{1/2}^{-1})_{\pi}$  in  $^{39}\text{K}$  calculated using the H-F single-particle wave functions. The dashed and solid curves correspond to the H-F transition density without and with the core-polarization effects, respectively. The experimental data are taken from (Ref 20) (triangles) and (Ref 21) (circles).

Fig. (3) The proton transition densities of giant resonances. The solid curve shows that of IS resonance at  $E_x = 16.7$  MeV, while the dashed curve corresponds to the IV resonance at  $E_x = 29$  MeV. The magnitude of the transition density is determined by Eqs. (8) and (9) with the energy intervals  $E_x = 16.2$ -17.2 MeV for IS and  $E_x = 28.0$ -30.0 MeV for IV. The dotted curve is the transition density of the Tassie model Eq. (22) with an arbitrary scale.

Fig. (4) The transition densities  $\rho_{\rho}^{\lambda=2}$  for the

$(0d_{3/2}^{-1} \rightarrow 1s_{1/2}^{-1})_{\pi}$  excitation at  $E_x = 2.53$  MeV

in  $^{39}\text{K}$ . The dashed and solid curves correspond to without and with the core polarization, respectively. For comparison we also show the transition density for the IS resonance from Fig. (3) (the dashed curve in this figure).

Fig. (5) The transverse form factor of the transition  $(0d_{3/2}^{-1} \rightarrow 1s_{1/2}^{-1})_{\pi}$ . The dotted curve corresponds to the M1 form factor, and the x sign corresponds to the E2 form factor without core polarization. The sum of M1 and E2 form factors are shown by the dashed curve (without core polarization) and the solid curve (with core polarization). The experimental data are taken from (Ref 21).

## References:

1. B. A. Brown, R. Radhi and B. H. Wildenthal, physics Reports 101 315 (1983).
2. T. Iwamoto, H. Horie and A. Yokoyama, Phys. Rev. C25, 658 (1982).
3. J. Heisenberg, J. Dawson, T. Millman, O. Schwenker, J. Lichtenstadt, C. N. Papanicolas, J. Wise, J. S. McCarthy, N. Hintz and H. P. Blok, Phys. Rev. C29, 97 (1984).
4. A. Bohr and B. R. Mottelson, Nuclear Structure Vol. II (New York, Benjamin, 1979).
5. Y. Horikawa, T. Hoshino and A. Arima, Nucl. Phys. A278, 297 (1977)
6. F. Petrovich, H. Mcmannus, J. Borysowicz and G. R. Hammerstein, Phys. Rev. C16, 839 (1977)
7. I. Hamamoto, Phys. Reports, 10C, 1 (1974)
8. T. Suzuki, Nucl. Phys. A217, 182 (1973); A220, 569 (1974)
9. Nguyen van Giai and H. Sagawa, Nucl. Phys. A371, 1 (1981)
10. Nguyen van Giai and H. Sagawa, Phys. Lett. 106B, 379 (1981)
11. G. F. Bertsch and S. F. Tsai, Phys. Reports 18, 125 (1975)
12. S. Sholomo and G. F. Bertsch, Nucl. Phys. A243, 307 (1975)
13. A. Bohr and B. R. Mottelson, Nuclear Structure Vol. I (New York, Benjamin, 1975).
14. H. Sagawa, Phys. Rev. C19, 506 (1979)
15. A. van der Woude et al., Contrib. to Florence Int. Conf. on Nucl. Structure (Florence, 1983) p.241
16. H. Krivine, J. Treiner and O. Bohigas, Nucl. Phys. A336, 155 (1980).
17. B. A. Brown, A. Arima and J. B. McGroory, Nucl. Phys. A277, 77 (1977).
18. B. A. Brown, B. H. Wildenthal, W. Chung, S. E. Massen, M. Benas, A. M. Bernstein, R. Miskimen, V. R. Brown and V. A. Madsen, Phys. Rev. C26, 2247 (1982).
19. L. Zamick, M. Golin and S. Moszkowski, Phys. Lett. 66B, 116 (1977)
20. TH. Grundy, A. Richter, G. Schrieder, E. Spamer and W. Stock, Nucl. Phys. A357, 269 (1981).
21. C. W. de Jager, P. H. M. Keizer, S. W. Kowalski, L. Lapikas, E. A. J. M. Offermann and H. de Vries, Proceedings of the International Conference on Nuclear Physics, Volume 1, Contributed Papers, Florence, 1983 and private communication.
22. L. J. Tassie and F. C. Barker, Phys. Rev. 111, 940 (1958).
23. H. D. Wohlfahrt, E. B. Shera, M. V. Hoehn, Y. Yamazaki and R. M. Steffen, Phys. Rev. C23, 533 (1981).
24. I. S. Towner and F. C. Khanna, Nucl. Phys. A399, 334 (1983).



Table I

Isoscalar contribution to the core-polarization charges for the 0s-1d particle states in  $^{16}\text{O}$  and hole states in  $^{40}\text{Ca}$

f	i	$^{16}\text{O}$ $\pi$ ( $\gamma$ )	$^{40}\text{Ca}$ $\pi$ ( $\gamma$ )
0d3/2	0d3/2	0.155 (0.176)	0.406 (0.396)
0d3/2	0d5/2	0.269 (0.288)	0.473 (0.465)
1s1/2	0d3/2	0.151 (0.168)	0.450 (0.436)
0d5/2	0d5/2	0.359 (0.361)	0.423 (0.413)
1s1/2	0d5/2	0.251 (0.265)	0.495 (0.489)

Table III

Isoscalar (IS) and isovector (IV) contributions to the core-polarization charges for the 1s-0d hole states in  $^{40}\text{Ca}$ . The individual IS and IV results for protons and neutrons only differ by a few percent and hence only the average is given here. The proton and neutron core-polarization charges given are the total of the IS and IV contributions.

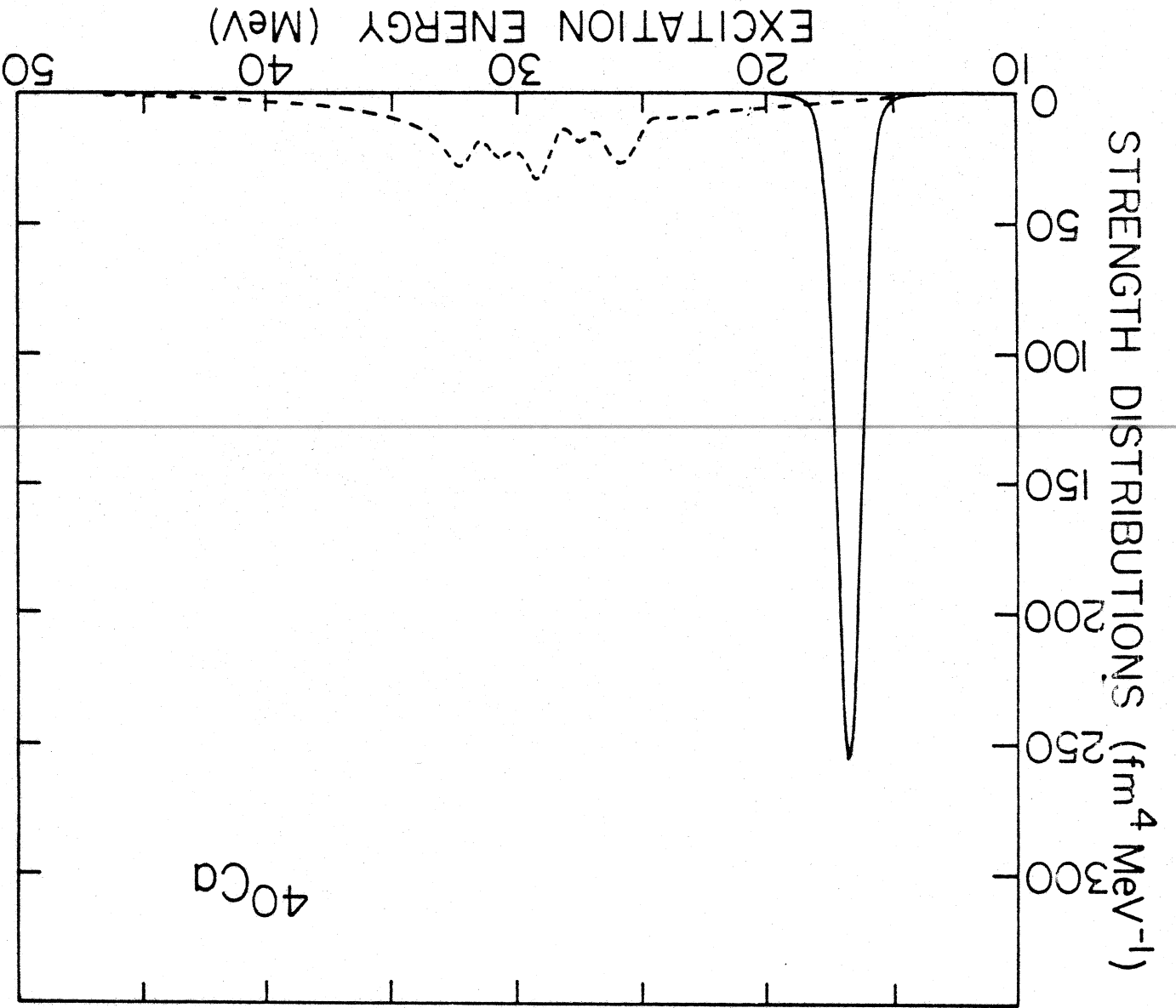
f	i	IS	IV	$\pi$	$\gamma$
0d3/2	0d3/2	0.401	0.110	0.291	0.511
0d3/2	0d5/2	0.469	0.119	0.350	0.588
1s1/2	0d3/2	0.443	0.101	0.342	0.544
0d5/2	0d5/2	0.418	0.117	0.301	0.535
1s1/2	0d5/2	0.492	0.108	0.384	0.600

Table II

The values of G defined by Eq. (21) for the configurations involved in the 0s-1d shell E2 transitions. For the harmonic-oscillator radial wave functions values of  $b=1.769$  fm for  $^{16}\text{O}$  and  $b=1.963$  fm for  $^{40}\text{Ca}$  were used.

f	i	$^{16}\text{O}$ $\pi$ ( $\gamma$ )	$^{40}\text{Ca}$ $\pi$ ( $\gamma$ )
0d3/2	0d3/2	1.936 (1.524)	1.002 (0.965)
0d3/2	0d5/2	1.198 (1.114)	0.979 (0.948)
1s1/2	0d3/2	1.882 (1.535)	0.991 (0.949)
0d5/2	0d5/2	1.027 (0.981)	0.962 (0.935)
1s1/2	0d5/2	1.183 (1.091)	0.950 (0.918)

Figure 1



$^{40}\text{Ca}$

MSU-84-057

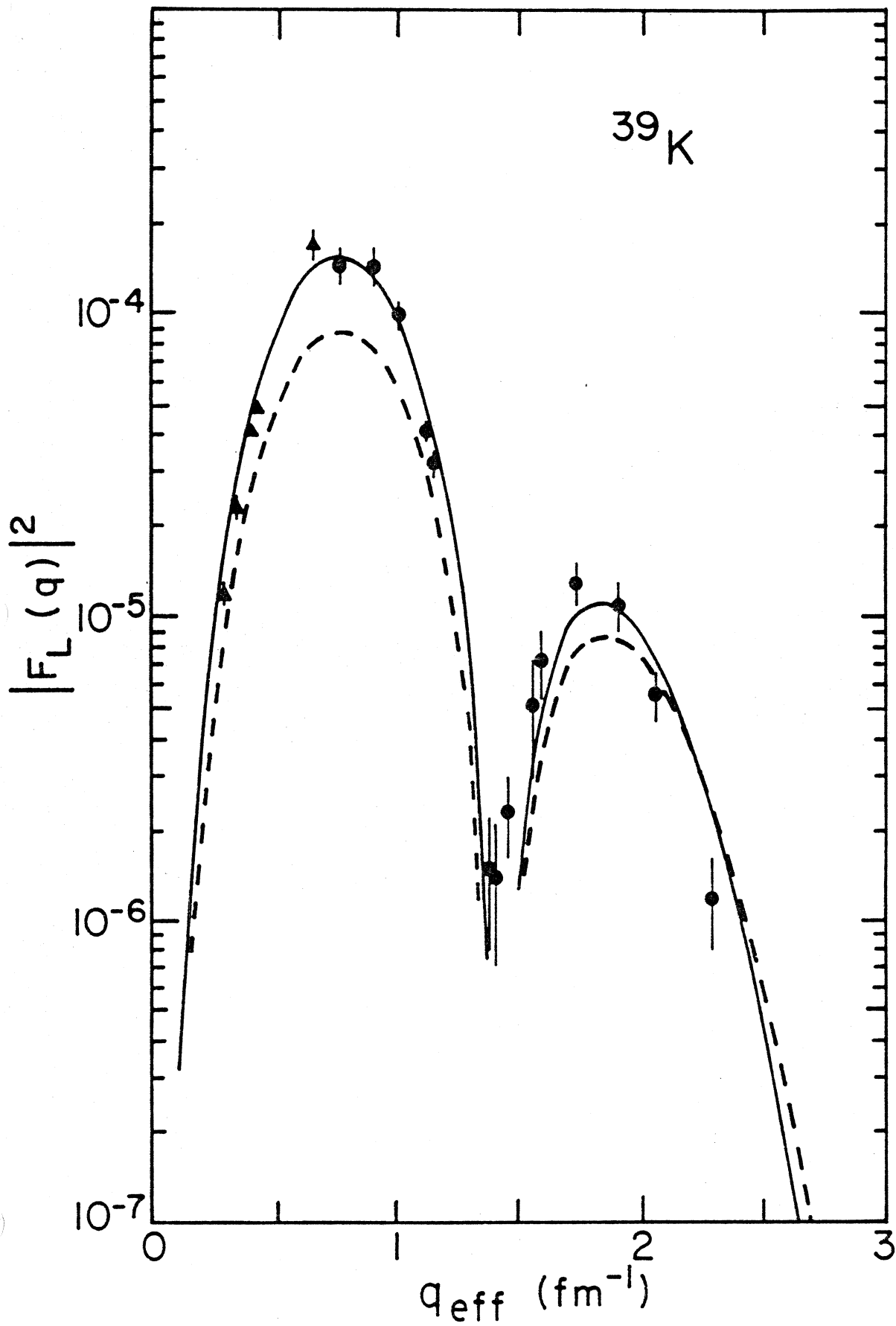
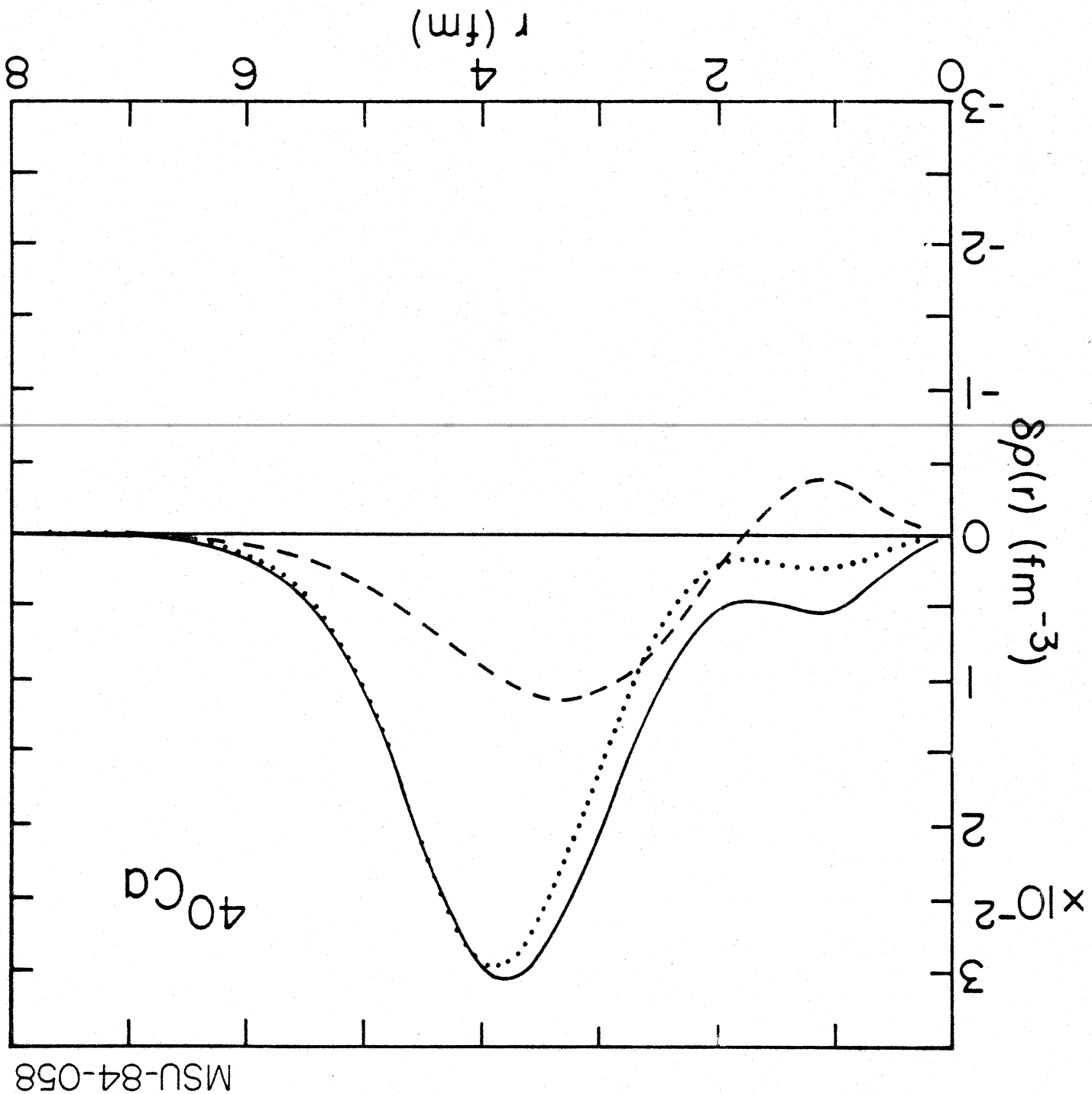


Figure 2

Figure 3



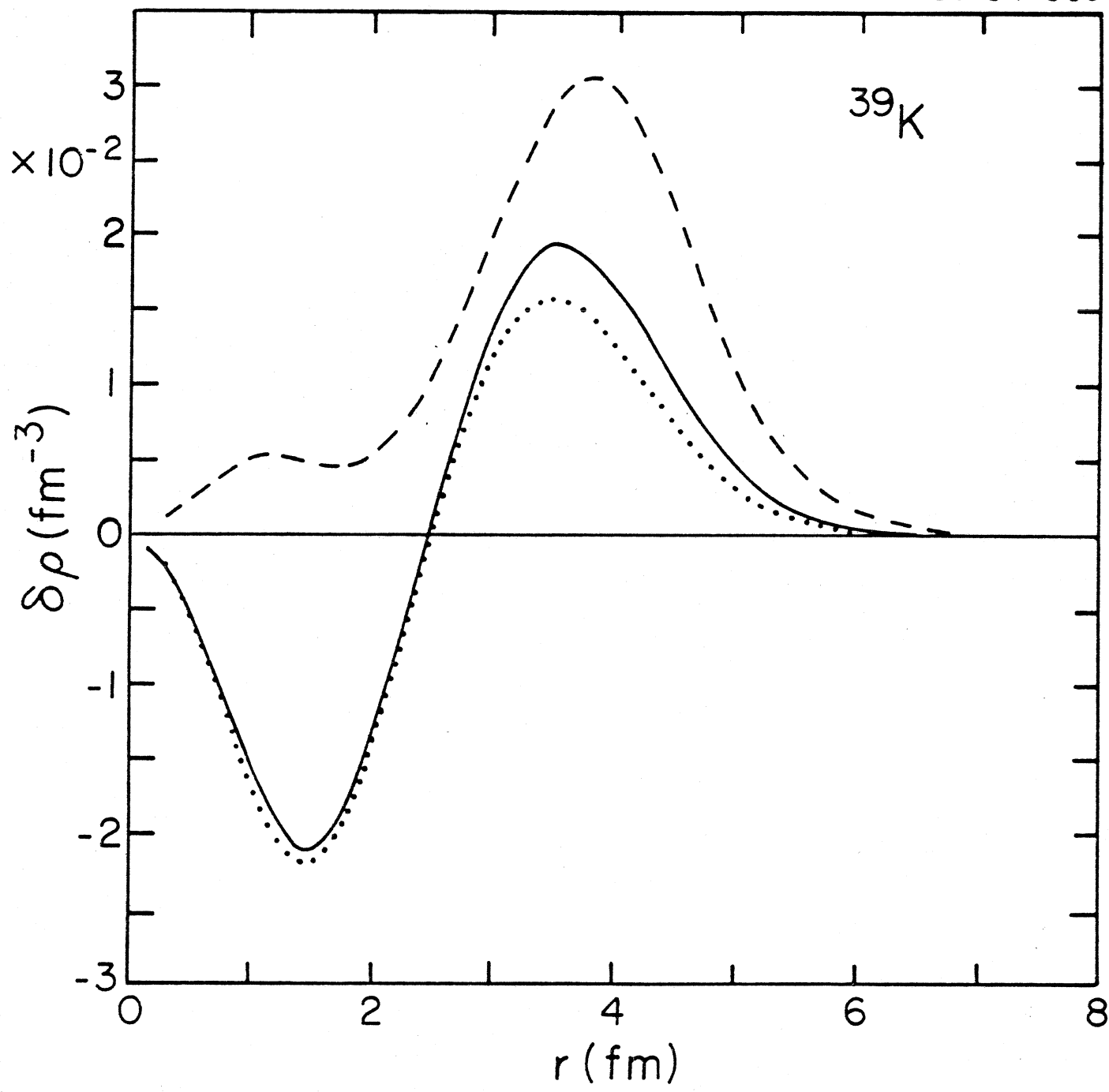


Figure 4

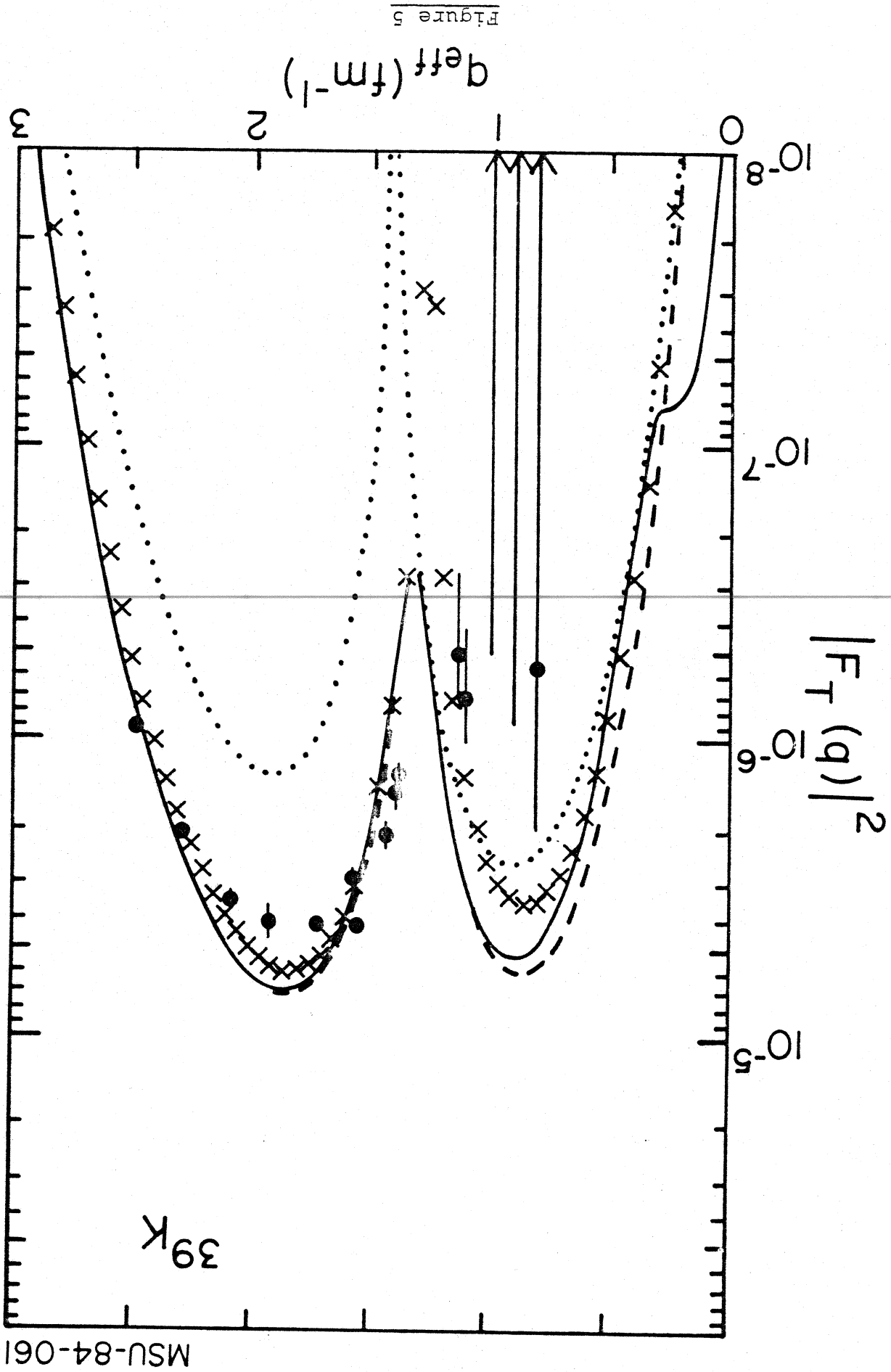


Figure 5

MSU-84-061

$^{39}\text{K}$